



Article

Formation of Micro and Mesoporous Amorphous Silica-Based Materials from Single Source Precursors

Mohd Nazri Mohd Sokri ^{1,2}, Yusuke Daiko ^{1,3}, Zineb Mouline ¹, Sawao Honda ^{1,3} and Yuji Iwamoto ^{1,3,*}

¹ Department of Frontier Materials, Graduate School of Engineering, Nagoya Institute of Technology, Gokiso-cho, Showa-ku, Nagoya 466-8555, Japan; nazrisokri@utm.my (M.N.M.S.); daiko.yusuke@nitech.ac.jp (Y.D.); zinebmln@gmail.com (Z.M.); honda@nitech.ac.jp (S.H.)

² Department of Energy Engineering and Advanced Membrane Technology Research Centre, Faculty of Chemical and Energy Engineering, Universiti Teknologi Malaysia (UTM), Johor Bahru 81310, Malaysia

³ Core Research for Evolutional Science and Technology (CREST), Japan Science and Technology Agency, Gokiso-cho, Showa-ku, Nagoya 466-8555, Japan

* Correspondence: iwamoto.yuji@nitech.ac.jp; Tel./Fax: +81-52-735-5276

Academic Editors: Samuel Bernard, André Ayril and Philippe Miele

Received: 8 January 2016; Accepted: 1 March 2016; Published: 9 March 2016

Abstract: Polysilazanes functionalized with alkoxy groups were designed and synthesized as single source precursors for fabrication of micro and mesoporous amorphous silica-based materials. The pyrolytic behaviors during the polymer to ceramic conversion were studied by the simultaneous thermogravimetry-mass spectrometry (TG-MS) analysis. The porosity of the resulting ceramics was characterized by the N₂ adsorption/desorption isotherm measurements. The Fourier transform infrared spectroscopy (FT-IR) and Raman spectroscopic analyses as well as elemental composition analysis were performed on the polymer-derived amorphous silica-based materials, and the role of the alkoxy group as a sacrificial template for the micro and mesopore formations was discussed from a viewpoint to establish novel micro and mesoporous structure controlling technologies through the polymer-derived ceramics (PDCs) route.

Keywords: perhydropolysilazane; alkyl alcohol; single source precursor; polymer-derived ceramics; micro and mesoporous silica

1. Introduction

The organometallic precursor route has received increased attention as an attractive ceramic processing method since it has inherent advantages over conventional powder processing methods such as purity control, compositional homogeneity in the final ceramic product and lower processing temperatures in the ceramics fabrication [1–3]. Moreover, this route provides alternatives towards the synthesis of advanced silicon-based non-oxide ceramics such as silicon nitride (Si₃N₄)-based ceramics, particularly starting from silicon-based polymers such as polysilazanes [4–6].

Recently, micro and mesoporous structure formations have been often discussed for the polymer-derived amorphous silicon nitride [7,8], silicon carbide [9–14], silicon carbonitride (Si–C–N) [15], silicon oxycarbide (Si–O–C) [16–18] and quaternary Si–M–C–N (M = B [19,20], Ni [21]). During the crosslinking and subsequent high-temperature pyrolysis under an inert atmosphere of polymer precursors, by-product gases such as CH₄, NH₃ and H₂ were detected [5,22], and the microporosity in the polymer-derived non-oxide amorphous ceramics could be assigned to the release of the small gaseous species formed *in-situ* [8,22].

Iwamoto *et al.* [23] reported an approach in synthesizing micro and mesoporous amorphous silica using organo-substituted polysilazane precursors, in which the organic moieties acted as a “sacrificial

template” during polymer to ceramic conversion by heat treatment in air, thus allowing the micro and mesoporous structure formation.

In our recent studies, commercially available perhydropolysilazanes (PHPS) was used as a starting polymer. The PHPS contains many reactive Si–H and N–H groups which can react with chemical modifiers to yield novel ternary or quaternary Si-based non-oxide ceramics [24–27]. In addition, compared with polysiloxanes often used as a precursor for silica, PHPS can be easily oxidized at low temperatures to yield pure silica in high ceramic yield due to the weight gain as shown in the following equation [28–30].



In our previous studies, alkoxy groups were introduced to PHPS, and the resulting chemically modified PHPS was converted to microporous amorphous silica by oxidative crosslinking at 270 °C followed by heat treatment at 600 °C in air (route R1 in Figure 1) [31]. Microporous amorphous silica was also synthesized through the two step conversion route, (i) room temperature oxidation of the chemically modified PHPS to afford an air-stable alkoxy group-functionalized amorphous silica-based inorganic-organic hybrid; and (ii) subsequent heat treatment at 600 °C in air (route R2 in Figure 1) [32]. In continuation of our ongoing studies, we herein report the effect of the heat treatment atmosphere on porous structure development of the polymer-derived amorphous silica-based materials. The polymer/ceramics thermal conversion under an argon flow was performed on the polymer precursors and the polymer-derived hybrid silica (route R3 and R4 in Figure 1). The thermal conversion behaviors were *in-situ* analyzed by the simultaneous thermogravimetry-mass spectrometry (TG-MS) analysis. The relationships between the heat treatment atmosphere, gaseous species formed *in-situ* during the thermal conversion and the micro and mesoporosity in the resulting amorphous silica-based materials are discussed and compared with our previous results [32] in order to achieve a better understanding of the micro and mesoporous structure development in the polymer-derived amorphous-silica based materials.

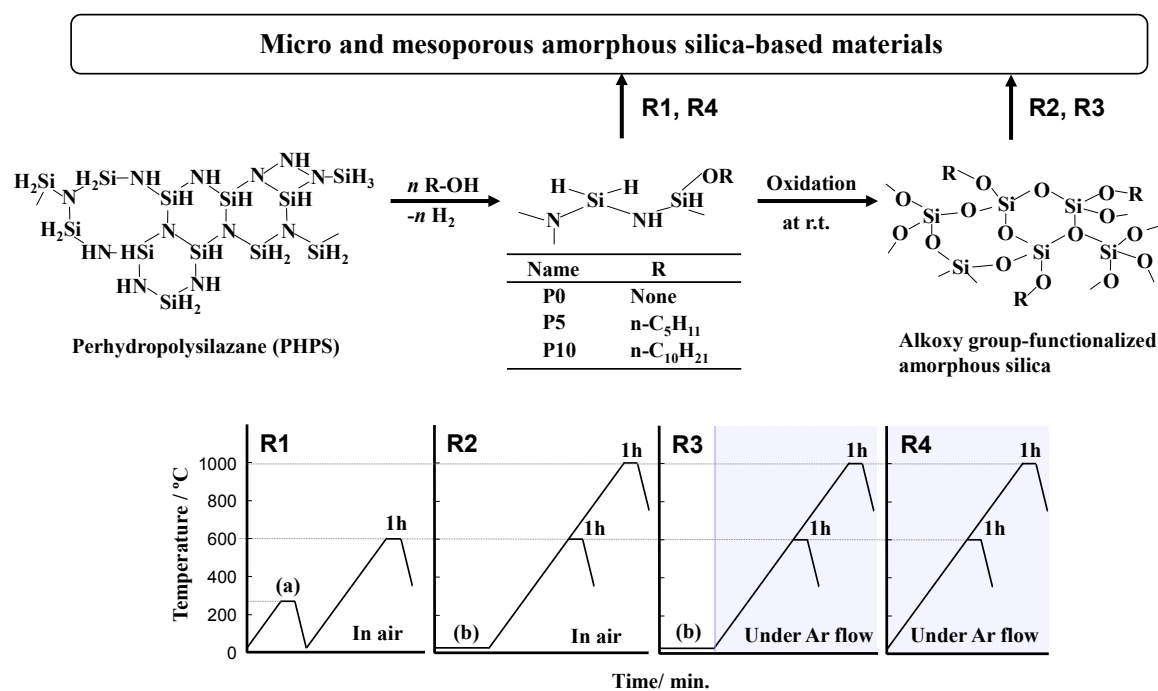


Figure 1. Synthesis of micro- and mesoporous amorphous silica-based materials through polymer derived ceramics (PDCs) routes investigated in this study.

2. Results and Discussion

2.1. Polymer Precursors and Alkoxy Group-Functionalized Amorphous Silica

The chemical structures of the polymer precursors and those of the alkoxy group-functionalized inorganic-organic hybrid silica were assessed based on their FT-IR spectra. As shown in Figure 2a, the as-received PHPS exhibited absorption bands at 3400 (ν N–H), 2150 (ν Si–H), 1180 (δ N–H) and 840–1020 cm^{-1} (δ Si–N–Si) [4,31–33]. The PHPSs modified with the alcohols (Figure 2b,c) presented additional absorption bands at 2950–2850 (ν C–H), 1450 (δ CH₃) and 1090 cm^{-1} (ν Si–OR) [31,32,34]. As shown in Figure 2a, after the room temperature oxidation, the absorption bands corresponding to the as-received PHPS completely disappeared and new absorption bands appeared at 3400 (Si–OH) and 1090 cm^{-1} (Si–O–Si) [32,34]. In addition to these bands, the chemically modified PHPSs exhibited C–H absorption bands in the vicinity of 2950 to 2850 cm^{-1} (Figure 2b,c).

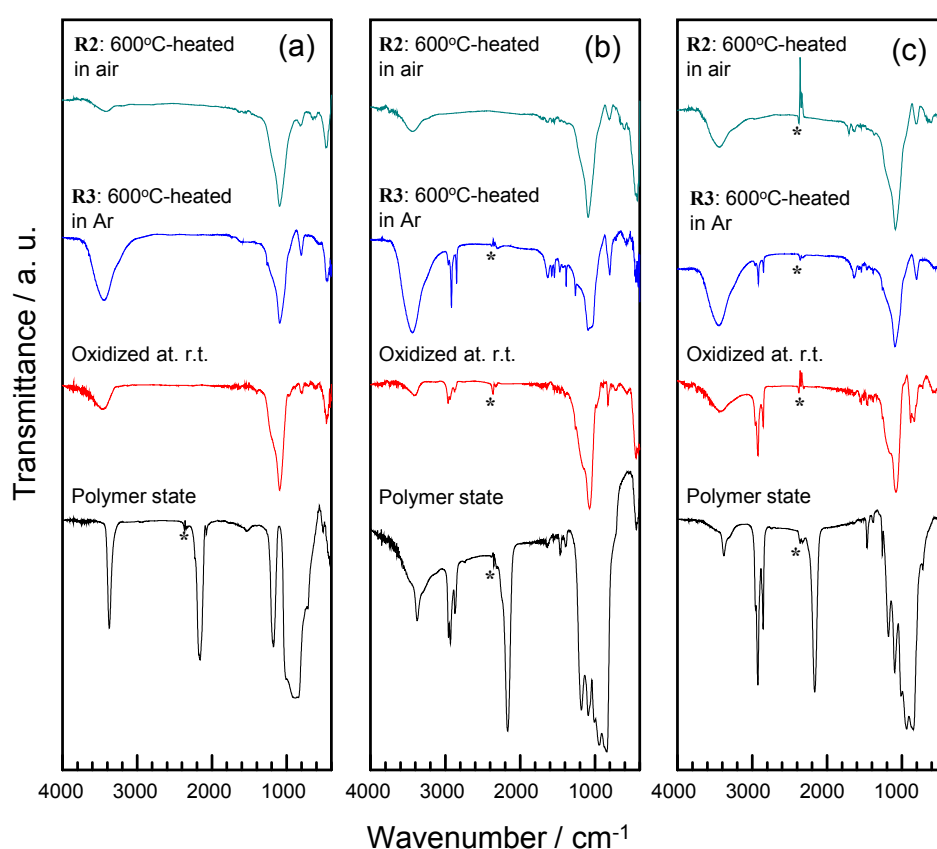


Figure 2. FT-IR spectra for polymer precursors and the precursor-derived samples. Polymer precursor: (a) P0; (b) P5 and (c) P10 (* indicating background, absorption due to CO₂).

The chemical structure of the oxidized samples was further studied by the solid state ²⁹Si magic angle spinning (MAS) NMR spectroscopy. As a typical result, the spectrum for the sample derived from PHPS chemically modified with *n*-C₁₀H₂₁OH (P10) is shown in Figure 3. The characteristic peaks due to the structural units of as-received PHPS at around –35 ppm (SiHN₃/SiH₂N₂) and –50 ppm (SiH₃N) [35] completely disappeared, and the spectrum presented new broad peaks assigned to the units which composed amorphous silica at –78, –89, –85 to –94 and –112 ppm assigned to Q1(≡SiO–SiX₃), Q2 ((≡SiO)₂SiX₂), Q3 ((≡SiO)₃SiX) and Q4 ((≡SiO)₄Si) (X = OH, OC₁₀H₂₁), respectively. These results indicate that the as-received PHPS and the chemically modified PHPSs were successfully converted to amorphous silica, and alkoxy group-functionalized inorganic-organic hybrid silica, respectively.

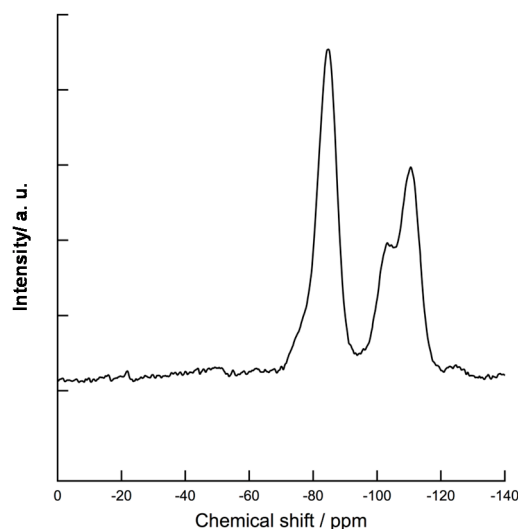


Figure 3. ^{29}Si MAS NMR spectrum for alkoxy group-functionalized amorphous silica synthesized by room temperature oxidation of **P10** (PHPS chemically modified with $n\text{-C}_{10}\text{H}_{21}\text{OH}$).

2.2. Thermal Conversion to Amorphous Silica-Based Materials

The oxidative cross-linking at 270 °C and subsequent heat treatment at 600 °C in air of the polymer precursors (route R1) yielded carbon-free amorphous silica (Table 1, route R1, 600 °C). The alkoxy group-functionalized inorganic-organic hybrid silica could be also converted to carbon-free amorphous silica by the 600 °C-heat treatment in air (Table 1, route R2, 600 °C), and the C–H absorption bands completely disappeared in their FT-IR spectra (R2 in Figure 2b,c). On the other hand, the 600 °C-heat treatment in argon (Ar) resulted in the detection of C–H absorption bands (R3 in Figure 2b,c). The amount of carbon remained in the **P5** and **P10**-derived samples were 6.2 and 9.5 wt %, respectively (Table 1, route R3, 600 °C).

Table 1. Chemical composition of polymer-derived amorphous silica-based materials synthesized in this study.

Polymer	Conversion Route	Flow Gas	Temp./°C	Composition/wt %					Empirical Ratio
				Si	C	O	N	H	
P0	R1	air	600	68.1	0.0	30.2	0.7	0.0	$\text{Si}_{1.0}\text{C}_{0.00}\text{O}_{0.78}\text{N}_{0.02}\text{H}_{0.00}$
	R2	air	600	59.1	0.0	39.3	0.6	0.0	$\text{Si}_{1.0}\text{C}_{0.00}\text{O}_{1.17}\text{N}_{0.02}\text{H}_{0.00}$
	R3	Ar	600	54.5	0.0	42.4	1.9	0.2	$\text{Si}_{1.0}\text{C}_{0.00}\text{O}_{1.37}\text{N}_{0.07}\text{H}_{0.10}$
	R4	Ar	600	65.8	0.9	4.8	26.9	0.6	$\text{Si}_{1.0}\text{C}_{0.03}\text{O}_{0.13}\text{N}_{0.82}\text{H}_{0.25}$
	R3	Ar	1000	58.1	0.0	40.2	0.5	0.2	$\text{Si}_{1.0}\text{C}_{0.00}\text{O}_{1.21}\text{N}_{0.02}\text{H}_{0.10}$
	R4	Ar	1000	63.4	0.9	5.0	29.1	0.6	$\text{Si}_{1.0}\text{C}_{0.03}\text{O}_{0.14}\text{N}_{0.92}\text{H}_{0.26}$
P5	R1	air	600	64.7	0.0	34.2	0.1	0.0	$\text{Si}_{1.0}\text{C}_{0.00}\text{O}_{0.93}\text{N}_{0.003}\text{H}_{0.00}$
	R2	air	600	60.7	0.0	38.2	0.1	0.0	$\text{Si}_{1.0}\text{C}_{0.00}\text{O}_{1.10}\text{N}_{0.003}\text{H}_{0.00}$
	R3	Ar	600	55.6	6.2	36.2	0.6	0.4	$\text{Si}_{1.0}\text{C}_{0.26}\text{O}_{1.13}\text{N}_{0.02}\text{H}_{0.20}$
	R3	Ar	1000	52.7	4.1	41.8	0.3	0.1	$\text{Si}_{1.0}\text{C}_{0.18}\text{O}_{1.39}\text{N}_{0.01}\text{H}_{0.05}$
P10	R1	air	600	64.7	0.0	34.3	0.0	0.0	$\text{Si}_{1.0}\text{C}_{0.00}\text{O}_{0.93}\text{N}_{0.00}\text{H}_{0.00}$
	R2	air	600	63.1	0.0	35.9	0.0	0.0	$\text{Si}_{1.0}\text{C}_{0.00}\text{O}_{1.00}\text{N}_{0.00}\text{H}_{0.00}$
	R3	Ar	600	51.9	9.5	36.6	0.1	0.9	$\text{Si}_{1.0}\text{C}_{0.43}\text{O}_{1.24}\text{N}_{0.004}\text{H}_{0.48}$
	R4	Ar	600	57.7	6.7	30.2	3.0	1.4	$\text{Si}_{1.0}\text{C}_{0.27}\text{O}_{0.92}\text{N}_{0.10}\text{H}_{0.68}$
	R2	air	1000	63.6	0.0	35.4	0.0	0.0	$\text{Si}_{1.0}\text{C}_{0.00}\text{O}_{0.98}\text{N}_{0.00}\text{H}_{0.00}$
	R3	Ar	1000	49.4	6.1	42.3	0.0	1.2	$\text{Si}_{1.0}\text{C}_{0.29}\text{O}_{1.50}\text{N}_{0.00}\text{H}_{0.68}$
	R4	Ar	1000	59.6	8.4	14.9	14.4	1.7	$\text{Si}_{1.0}\text{C}_{0.33}\text{O}_{0.44}\text{N}_{0.48}\text{H}_{0.79}$

2.3. TG-MS Analysis

To study the effect of atmosphere on the pyrolytic behaviors more extensively, TG-MS analysis was performed on the selected samples. The results were summarized and shown in Figures 4 and 5. The PHPS-derived amorphous silica synthesized by the room temperature oxidation showed a slight weight loss at 150 to 400 °C (Figure 4(Aa)). The MS spectrum measured at 200 °C was composed of m/z ratios at 106, 91, 77, 63, 51 and 39, which was identical to that reported for xylene (Figure 4(Ab)) [36,37]. Since the molecular ion ($m/z = 106$) and the tropylium ion ($m/z = 91$) were detected at 400 °C and below (Figure 4(Ac)), the observed weight loss is mainly due to the residual xylene [32]. When the PHPS was directly heat-treated under the inert atmosphere, the weight loss up to 400 °C increased to approximately 20 wt % (Figure 4(Ba)). A typical MS spectrum measured at 200 to 250 °C is shown in Figure 4(Bb). The m/z ratios at 76 and 30 were assigned to $\text{SiH}_2\text{-NH-SiH}_3^+$ and SiH_2^+ , respectively. The smaller species, m/z ratios at 28 and 17 were assigned to N_2^+ and NH_3^+ , respectively. These fragment ions could be formed *in-situ* by the thermal decomposition of the silazane rings. The evolutions of these gaseous species were found to be completed at around 400 °C (Figure 4(Bc)).

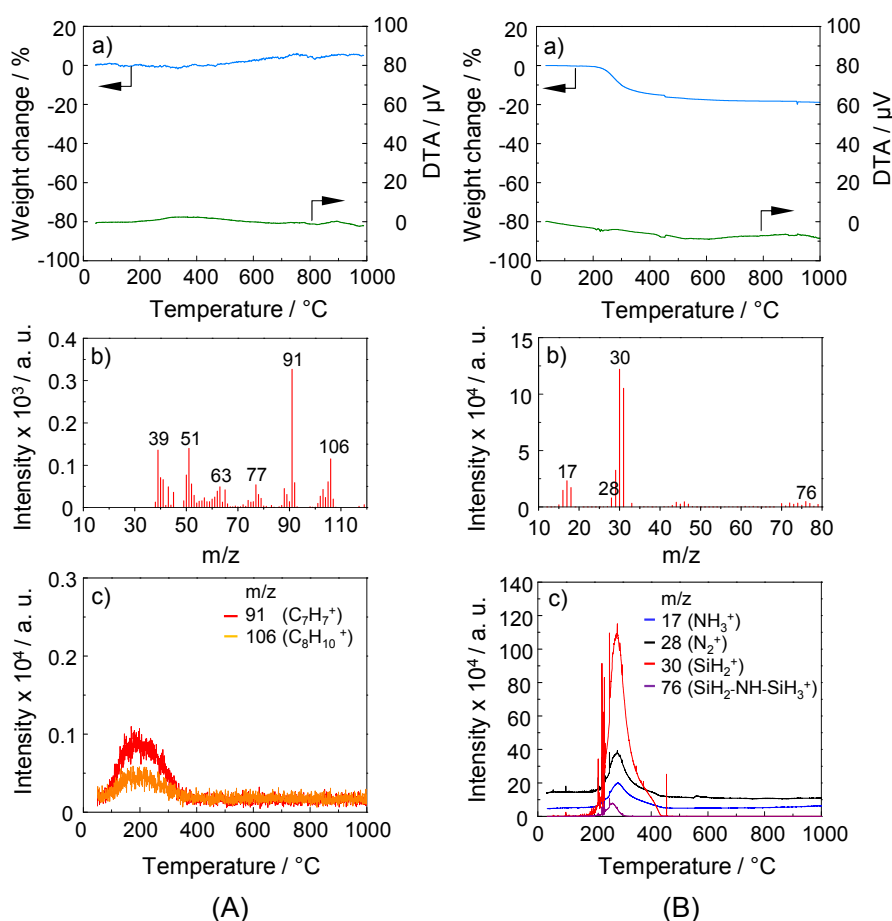


Figure 4. Thermal behavior of (A) PHPS (P0)-derived amorphous silica under oxidative atmosphere (route R2); and (B) as-received PHPS under an inert atmosphere (route R4). (a) TG-DTA; (b) monitoring of gaseous species by mass spectrometry at 200 °C and (c) continuous *in-situ* monitoring of gaseous species by mass spectrometry.

As shown in Figure 5(Aa), under the oxidative atmosphere (route R2), the P10-derived hybrid silica having $n\text{-C}_{10}\text{H}_{21}\text{O}$ groups exhibited a weight loss of approximately 50% at 150 to 600 °C, and the differential thermal analysis (DTA) resulted in the detection of a dominant exothermic peak centered at 320 °C. The MS spectrum measured at 320 °C is shown in Figure 5(Ab). The sequential peaks 14 mass

units apart at $m/z = 71, 57$ and 43 can be assigned to the fragment ions derived from hydrocarbons formed *in situ* by the typical α -cleavage in the n -C₁₀H₂₁O group, followed by the sequential C–C bond cleavage to release methylene units [36,38]. The m/z ratios at $m/z = 70$ (C₅H₁₀^{•+}) and 55 (C₄H₇⁺) could be derived from traces of unreacted n -C₁₀H₂₁OH [36,39]. The smaller species, m/z ratios at 44 and 18 were assigned to CO₂⁺ and H₂O⁺, respectively. By monitoring the fragment ions with m/z ratios at $85, 71, 57$ and 43 , it was confirmed that the decomposition of n -C₁₀H₂₁O group mainly occurred at 250 to 500 °C (Figure 5(Ac)). Simultaneously, combustion of the hydrocarbon species started at around 250 °C, and the evolution of CO₂ and H₂O continued to approximately 650 °C (Figure 5(Ad)).

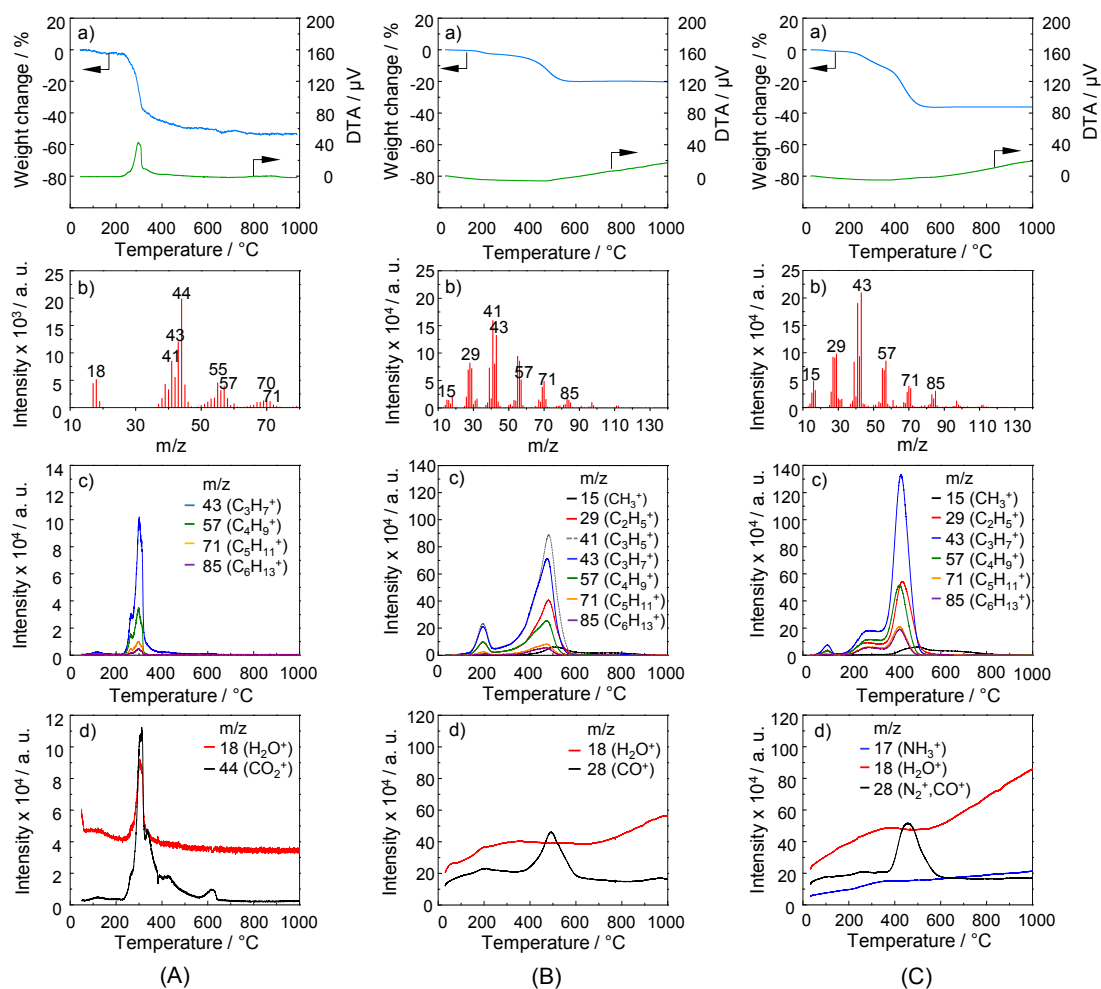


Figure 5. Thermal behavior of n -C₁₀H₂₁O group-functionalized hybrid silica under (A) oxidative atmosphere (route R2); (B) inert atmosphere (route R3) and (C) that of P10 functionalized with n -C₁₀H₂₁O groups (P10) under inert atmosphere (route R4). (a) TG-DTA; (b) monitoring of gaseous species by mass spectrometry at 320 °C; (c,d) continuous *in situ* monitoring of gaseous species by mass spectrometry.

Under the inert atmosphere (route R3) (Figure 5(Ba)), the weight loss up to 600 °C of the P10-derived hybrid silica was decreased to 20%. The MS spectrum measured at 320 °C was composed of the above mentioned species derived from n -C₁₀H₂₁O groups and those with the m/z ratios of 41 (C₃H₅⁺), 29 (C₂H₅⁺) and 15 (CH₃⁺) (Figure 5(Bb)). The gaseous species formed *in situ* were detected mainly at 100 to 600 °C (Figure 5(Bc)). When the P10 was directly heat-treated under an inert atmosphere (route R4), the weight loss up to 600 °C was rather suppressed and measured to be 38%. The thermal decomposition behavior of the P10 was similar to that characterized for the

n-C₁₀H₂₁O-functionalized hybrid silica, and it was found that the relative volume fraction of the *in situ* formed C₃H₇⁺ (*m/z* = 43) remarkably increased (Figure 5C).

2.4. N₂ Adsorption/Desorption Isotherm and Porosities Evaluated for the Polymer-Derived Amorphous Silica-Based Materials

The textural properties of the polymer-derived amorphous silica-based materials were studied by N₂ physisorption at −196 °C. The adsorption/desorption isotherms are presented in Figure 6. Each sample exhibited an N₂ uptake above $p/p_0 = 0.9$, which was thought to be related to the porosity generated by agglomeration of the powdered sample [31].

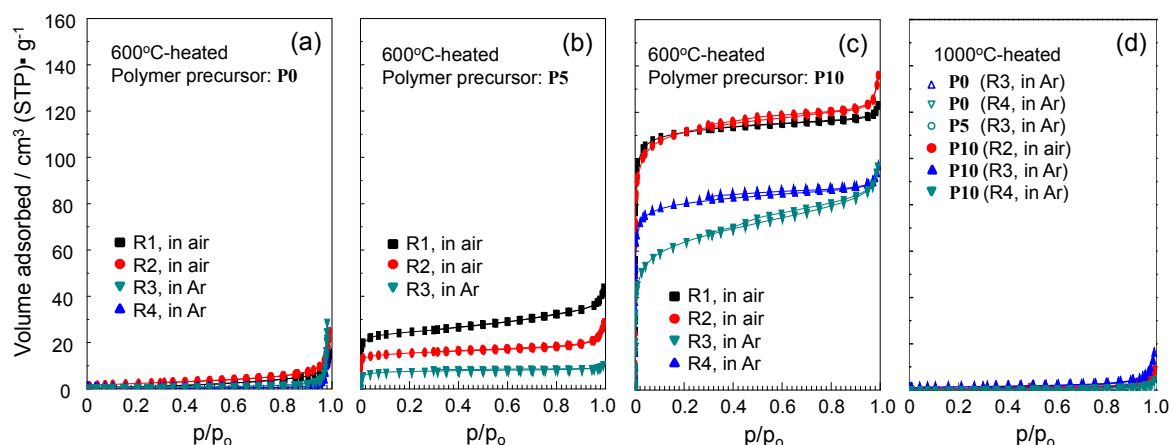


Figure 6. N₂ sorption isotherms of polymer-derived samples.

Regardless of the thermal conversion condition investigated in this study, the PHPS (P0)-derived amorphous silica generated a type III isotherm according to the International Union of Pure and Applied Chemistry (IUPAC) classification method [40,41] (Figure 6a), and the P0-derived samples were characterized as non-porous (Figure 7a). Consequently, it was clarified that the evolution below 400 °C of the relatively large gaseous species (shown in Figure 4) did not contribute to the porous structure formation.

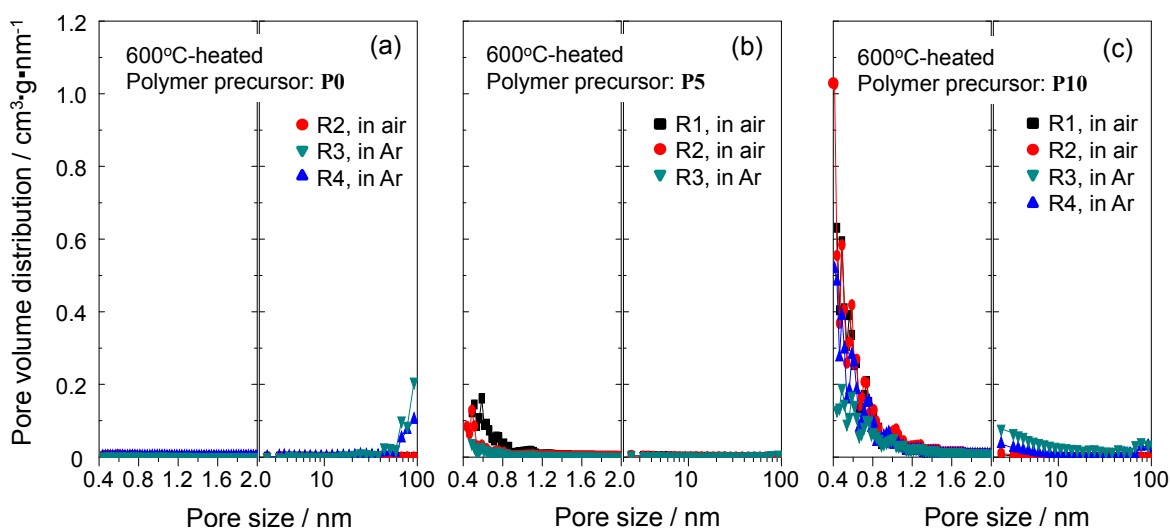


Figure 7. Pore size distribution of the polymer-derived samples synthesized by heat treatment at 600 °C for 1 h.

The isotherm of the **P5**-derived sample synthesized through the route R1 exhibited a type I without distinct hysteresis loops. The slight N_2 uptake at the relative pressure lower than $p/p_0 = 0.2$ was related to the micropore filling (Figure 6b), and the micropore sizes evaluated by using N_2 as probe molecule were in the range of 0.43 to 1.2 nm [31] (Figure 7b).

The isotherm of the **P10**-derived sample synthesized through the route R1 also presented a similar type (Figure 6c). The N_2 uptake below $p/p_0 = 0.2$ was apparently increased by increasing the carbon number in the alkoxy group from 5 to 10, and the resulting micropore size distribution plot peaked at 0.43 nm and extended to approximately 1.6 nm in size [31] (Figure 7c).

On the other hand, when the heat treatment of the **P5**-derived hybrid silica was performed under flowing Ar, the N_2 uptake below $p/p_0 = 0.2$ apparently decreased (R3 in Figure 6b). The micropore sizes evaluated for the resulting **P5**-derived sample were below 1.0 nm, and thus almost unchanged, while the micropore volume decreased (R3 in Figure 7b). In addition to the similar microporosity change (R3 in Figures 6c and 7c), the **P10**-derived sample exhibited an increase in the volume of mesopores having a size range of approximately 2 to 20 nm (R3 in Figure 7c).

The heat treatment under an Ar flow of the **P10** also resulted in the micro and mesoporosity changes similar to those observed for the **P10**-derived hybrid silica (R4 in Figures 6c and 7c). However, regardless of the atmospheric condition, the porosity in the **P5** and **P10**-derived samples was lost during further heat treatment from 600 to 1000 °C (Figure 6d).

Figure 8a presents the relations between the number of the carbon in the alkoxy group introduced to PHPS, the conversion route and the resulting micropore volume of the heat-treated samples. In our previous studies on the alkoxy group-functionalized PHPS [31] and hybrid silica [32], the alkoxy group with C3 hydrocarbon did not contribute to the porous structure development [31], while those having a carbon chain longer than or equal to C5 hydrocarbon were found to be effective as a sacrificial template for generating microporosity under the thermal conversion in air [32]. Moreover, the micropore volume increased with increasing the total volume of the released gaseous species having a kinetic diameter below 0.45 nm. As a result, the micropore volume of the **P10**-derived sample reached 0.17 cm³/g (R2 in Figure 8a), and this value was compatible with that of the amorphous silica fabricated without room temperature oxidation (route R1 in Figure 8a, 0.173 cm³/g). It should also be noted that the specific surface area (SSA) of this sample was 321.2 m²/g, and almost the same as that achieved by the sample fabricated through the route R1 (328 m²/g) [32].

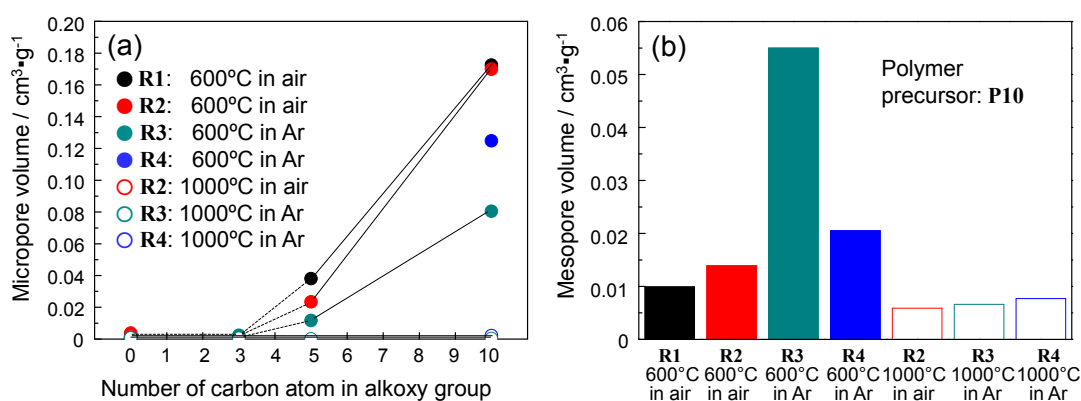


Figure 8. Porosity of polymer-derived amorphous silica-based materials. (a) micropore volume of the synthesized samples and (b) mesopore volume of **P10**-derived samples.

Under the present thermal conversion in Ar, the gaseous species formed *in situ* were C4–C1 hydrocarbons and CO with a kinetic diameter below 0.45 nm [42], which contributed to the microporosity formation in the **P5** and **P10**-derived samples. However, the total volume of the released gaseous species essentially decreased due to the lack of CO₂ evolution, which led to a decrease

in the micropore volume and a considerable amount of carbon remaining in the resulting amorphous silica-based material. Moreover, it was found that the decrease in the micropore volume became much more pronounced when the thermal conversion of **P10** was performed after the room temperature oxidation (R3 at the number of carbon = 10 in Figure 8a). Simultaneously, the mesopore volume in this sample turned out to be much higher ($0.055 \text{ cm}^3/\text{g}$) than those in other samples (approximately $0.01\text{--}0.02 \text{ cm}^3/\text{g}$) (Figure 8b). One possible reason for the decrease in the micropore volume associated with the increase in mesopore volume may be attributed to the pore growth from micro- to mesopore size range within the amorphous silica matrix immediately densified at the early stage of the heat treatment approximately below $400 \text{ }^\circ\text{C}$.

Figure 9 presents the Raman spectra for the **P10**-derived amorphous silica synthesized by heat treatment in air (route R2), and their assignments are listed in Table 2. The spectra for the $600 \text{ }^\circ\text{C}$ heat-treated sample exhibited broad bands related to the O–Si–O and Si–O–Si asymmetrical vibrations at 800 and 978 cm^{-1} , respectively [43]. The weak broad bands above 1000 cm^{-1} were thought to be attributed to the SiO_4 asymmetrical vibration [44–46]. On the other hand, the lower wavenumber bands below 700 cm^{-1} were attributed to the Si–O–Si symmetric vibrations originated from structural defects such as 3-, 4- and 6-membered Si–O–Si rings within the amorphous silica matrix [47–49].

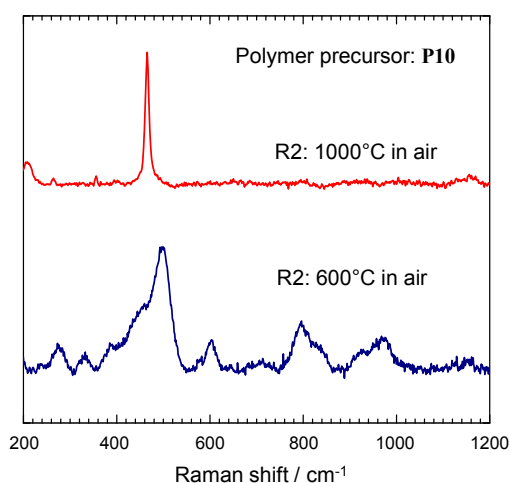


Figure 9. Raman spectra for **P10**-derived amorphous silica synthesized by heat treatment in air (route R2).

Table 2. Assignment for the Raman spectra shown in Figure 9.

ν , (Si–O–Si)/ cm^{-1}	Number of SiO_4 in Rings	Notes	Reference
381 (ν_s)	6	Observe in α -Carnegieite	Matson <i>et al.</i> [48]
463 (ν_s)	6	Observe in moganite	Kingma and Hemley [49]
465 (ν_s)	6	Observe in α -quartz	Kingma and Hemley [49]
498 (ν_s)	4 + 6	Observe in Leucite	Matson <i>et al.</i> [48]
606 (ν_s)	3	-	Uchino <i>et al.</i> [48]
800 (ν_{as})	-	O–Si–O vibration (asymmetric stretching mode)	Li <i>et al.</i> [43]
978 (ν_{as})	-	Si–O–Si bond due to defect by surface silanol group (asymmetric stretching mode)	Li <i>et al.</i> [43]
1000–1200 (ν_{as})	-	Asymmetric stretching SiO_4 vibrations	Apopei <i>et al.</i> [44] Makreski <i>et al.</i> [45] Ventura <i>et al.</i> [46]

On the other hand, after the high-temperature heat treatment up to $1000 \text{ }^\circ\text{C}$, the spectrum presented one distinct band at 465 cm^{-1} due to the six-membered Si–O–Si ring [49]. Since the intensity

of the characteristic bands related to the Si–O–Si and O–Si–O vibrations remarkably decreased, the 1000 °C heat-treated sample was thought to be composed of a highly rigid silica network.

It has been suggested that PHPS contains 2-, 3- and 4-membered Si–N–Si ring clusters as microporous units [5,22]. Upon oxidation at room temperature, the ring clusters were readily oxidized to form Si–O–Si linkages, which could serve as nucleation sites for subsequent growth of micropores. Finally, after the 1000 °C-heat treatment, the six-membered Si–O–Si rings remained to form the intrinsic microporosity in amorphous silica. The estimated diameter of the six-membered ring is approximately 0.3 nm [50,51], which is too small for the N₂ probe molecule to access (0.364 nm) [42]. Consequently, the resulting 1000 °C heat-treated sample was characterized as non-porous. On the other hand, the walls of micro- and mesopores formed by the thermal decomposition of the alkoxy groups are thought to be composed of disordered silica having considerable amount of dangling bonds, and the thermal stability of the polymer-derived micro- and mesoporous amorphous silica-based materials synthesized in this study is estimated to be around 600 °C.

3. Experimental Procedures

3.1. Precursor Synthesis

Commercially available perhydropolysilazane (PHPS, Type NN110, 20% xylene solution, AZ Electronic Materials, Tokyo, Japan) was used as the starting polymer. *n*-Pentanol (*n*-C₅H₁₁OH) and *n*-decanol (*n*-C₁₀H₂₁OH) were used for the chemical modification of the PHPS. According to the published procedures [32], the reaction between the as-received PHPS and each alcohol was carried out under a dry Ar atmosphere using Schlenk techniques. A PHPS (Si basis)/ROH molar ratio of 4:1 was applied in all cases. In each synthesis, the alcohol was added dropwise to a xylene solution of as-received PHPS with magnetic stirring at room temperature, followed by the addition of toluene to decrease the PHPS concentration from 20 to 1 wt %. After the addition was complete, the mixture was refluxed for 1 h under an Ar flow and cooled to room temperature. The xylene and toluene were removed from the reaction mixture under vacuum to afford the alcohol adduct as a viscous liquid.

3.2. Conversion of Polymer Precursor to Amorphous Silica-Based Materials

In this study, the polymer precursor was converted to amorphous silica-based material through the following four different routes shown in Figure 1.

R1: Oxidative crosslinking and subsequent heat treatment in air [31]

Polymer precursor was cured by heating at 270 °C in air to promote oxidative crosslinking with a heating rate of 100 °C/h and dwell time of 1 h in an alumina tube furnace. After cooling down to room temperature, the crosslinked polymer was obtained as white solid. The crosslinked polymer precursor was ground to a fine powder using a mortar and pestle, then heat-treated in an alumina tube furnace under an air flow by heating from room temperature to 600 °C in 6 h, maintaining the temperature at 600 °C for an additional 1 h, and finally cooling down to room temperature to give amorphous silica as white powders.

R2: Room temperature oxidation followed by heat treatment in air [32]

Polymer precursor was converted to amorphous silica-based hybrid by exposing the polymer precursor to vapour from aqueous ammonia (NH₃) according to the procedure reported by Kubo *et al.* [28,29]. In this process, 15 mL of aqueous NH₃ was placed in a 200 mL beaker with a slightly open lid and the polymer precursor (*ca.* 600 mg) was suspended over the aqueous NH₃ until the silica-based hybrid formed as white powder. The resulting amorphous silica-based hybrid was ground to a fine powder using a mortar and pestle, then heat-treated in an alumina tube furnace under an air flow up to 600 °C for a period of time of 6 h. Then the temperature was maintained at 600 °C for an additional hour, and finally cooled down to room temperature to afford amorphous silica as white powders.

R3: Room temperature oxidation followed by heat treatment in Ar

The powdered sample of polymer-derived amorphous silica-based hybrid was heat-treated in an alumina tube furnace under an Ar flow up to 600 °C at a heating rate of 10 °C/min. Then the temperature was maintained at 600 °C for an additional hour, and finally cooled down to room temperature.

R4: Heat treatment in Ar

Polymer precursor was heat-treated in an alumina tube furnace under Ar flow up to 600 °C for a period of time of 1 h (heating rate of 10 °C/min). Then the temperature was maintained at 600 °C for an additional 1 h, and finally cooled down to room temperature.

As shown in Figure 1, 1000 °C-heat treatment was also performed for the polymer/ceramics conversion (R2, R3 and R4).

3.3. Characterization

FT-IR spectra of the polymers and the polymer-derived amorphous silica-based materials were recorded using KBr pellets over the range of 4000 to 400 cm^{-1} (FT/IR-4200 IF, Jasco, Tokyo, Japan). Solid-state ^{29}Si magic angle spinning (MAS) nuclear magnetic resonance (NMR) spectra of the amorphous silica-based hybrids were measured at 79.45 MHz, 6.0 μs of 90° pulse length, 120 s of decay time between pulses, and spinning rate of 3500 Hz (Unity 400 plus, Varian, Palo Alto, CA, USA). Raman spectra of the amorphous silica-based materials were measured using 532 or 785 nm solid laser (Renishaw, Wotton-under-Edge, UK). The laser power of 5% was applied for the measurements.

The thermal behaviors up to 1000 °C were studied by simultaneous TG and MS analyses (Model TG/DTA6300, Hitachi High Technologies Ltd., Tokyo, Japan/Model JMS-Q1050GC, JEOL, Tokyo, Japan). The measurements were performed under flowing mixed gas of helium (He) and oxygen (O_2) (He: O_2 = 4:1, 100 mL/min) or He with a heating rate of 20 °C/min. To avoid the presence of dominant fragment peaks at around $m/z = 32$ (O_2^+) related to the presence of O_2 , the m/z ratios in the range of 20 to 35 were excluded from the MS spectra recorded under the flowing mixed gas of He and O_2 .

Elemental analyses were performed on the heat-treated samples for oxygen, nitrogen and hydrogen (inert-gas fusion method, Model EMGA-930, HORIBA, Ltd., Kyoto, Japan), and carbon (non-dispersive infrared method, Model CS744, LECO Co., St Joseph, MI, USA). The silicon content in the samples was calculated as the difference of the sum of the measured C, N, O and H content to 100 wt % [35].

The pore size distribution for the heat-treated samples was determined using a nitrogen (N_2) sorption technique with the relative pressure of the N_2 gas ranging from 0 to 0.99 (Belsorp Max, BEL Japan Inc., Osaka, Japan). The micropores ($r_{\text{pore}} < 2.0$ nm) and mesopores ($2.0 \text{ nm} \leq r_{\text{pore}} < 50$ nm) of the polymer-derived amorphous silica-based materials were characterized by the SF [52] and BJH [53] methods, respectively.

4. Conclusions

In this study, micro and mesoporous amorphous silica-based materials were successfully synthesized from single source precursors, PHPS functionalized with alkoxy groups (OR, R = $n\text{-C}_5\text{H}_{11}$, $n\text{-C}_{10}\text{H}_{21}$).

The textural properties evaluated for the polymer-derived amorphous silica-based materials suggested the potential of the polymer precursors employed in this study to develop a novel microporous structure controlling technology by manipulating the carbon chain in the alkoxy groups introduced to PHPS. It is also interesting to note that the PDC routes investigated in this study show some potential to synthesize mesoporous amorphous silica-based materials by the two-step conversion process, the room temperature oxidation followed by the thermal treatment under an inert atmosphere. These porous structure control technologies are expected to be useful to synthesize amorphous silica-based materials for energy application such as a highly efficient catalyst support and a gas separation membrane having a hyper-organized porous structure both in the micro- and mesopore size ranges.

Acknowledgments: This work was supported by CREST (Core Research for Evolutional Science and Technology) of Japan Science and Technology Corporation (JST).

Author Contributions: Mohd Nazri Mohd Sokri performed experiments and wrote the paper; Yusuke Daiko contributed NMR and FT-IR spectroscopic analyses; Sawao Honda contributed TG-MS analysis; Zineb Mouline contributed nitrogen adsorption/desorption measurements; Yuji Iwamoto conceived and designed experiments and wrote the paper.

Conflicts of Interest: The authors declare no conflict of interest.

References

1. Rice, R.W. Ceramics from polymer pyrolysis, opportunities and needs. A materials perspective. *Am. Ceram. Soc. Bull.* **1983**, *62*, 889–892.
2. Wynne, K.J.; Rice, R.W. Ceramics via polymer pyrolysis. *Annu. Rev. Mater. Sci.* **1984**, *14*, 297–334. [[CrossRef](#)]
3. Riedel, R.; Dressler, W. Chemical formation of ceramics. *Ceram. Int.* **1996**, *22*, 233–239. [[CrossRef](#)]
4. Seyferth, D.; Strohmam, C.; Dando, N.R.; Perrotta, A. Poly(ureidosilazanes): Preceramic polymeric precursors for silicon carbonitride and silicon nitride. Synthesis, characterization and pyrolytic conversion to Si₃N₄/SiC ceramics. *J. Chem. Mater.* **1995**, *7*, 2058–2066. [[CrossRef](#)]
5. Kroke, E.; Li, Y.-L.; Konetschny, C.; Lecomte, E.; Fasel, C.; Riedel, R. Silazane derived ceramics and related materials. *Mater. Sci. Eng. R* **2000**, *26*, 97–199. [[CrossRef](#)]
6. Funayama, O.; Arai, M.; Tashiro, Y.; Aoki, H.; Suzuki, T.; Tamura, K.; Kaya, H.; Nishii, H.; Isoda, T. Tensile strength of silicon nitride fibers produced from perhydropolysilazane. *J. Ceram. Soc. Jpn.* **1990**, *98*, 104–107. [[CrossRef](#)]
7. Miyajima, K.; Eda, T.; Ohta, H.; Ando, Y.; Nagaya, S.; Ohba, T.; Iwamoto, Y. Development of Si–N based hydrogen separation membrane. *Ceram. Trans.* **2010**, *213*, 87–94.
8. Schitco, C.; Bazarjani, M.S.; Riedel, R.; Gurlo, A. NH₃-assisted synthesis of microporous silicon oxycarbonitride ceramics from preceramic polymers: A combined N₂ and CO₂ adsorption and small angle X-ray scattering study. *J. Mater. Chem. A* **2015**, *3*, 805–818. [[CrossRef](#)]
9. Kusakabe, K.; Li, Z.Y.; Maeda, H.; Morooka, S. Preparation of supported composite membrane by pyrolysis of polycarbosilane for gas separation at high temperature. *J. Membr. Sci.* **1995**, *103*, 175–180. [[CrossRef](#)]
10. Li, Z.Y.; Kusakabe, K.; Morooka, S. Preparation of thermostable amorphous Si–C–O membrane and its application to gas separation at elevated temperature. *J. Membr. Sci.* **1996**, *118*, 159–168.
11. Nagano, T.; Sato, K.; Saito, T.; Iwamoto, Y. Gas permeation properties of amorphous SiC membranes synthesized from polycarbosilane without oxygen-curing process. *J. Ceram. Soc. Jpn.* **2006**, *114*, 533–538. [[CrossRef](#)]
12. Suda, H.; Yamauchi, H.; Uchimaru, Y.; Fujiwara, I.; Haraya, K. Preparation and gas permeation properties of silicon carbide-based inorganic membranes for hydrogen separation. *Desalination* **2006**, *193*, 252–255. [[CrossRef](#)]
13. Mourhatch, R.; Tsotsis, T.T.; Sahimi, M. Network model for the evolution of the pore structure of silicon-carbide membranes during their fabrication. *J. Membr. Sci.* **2010**, *356*, 138–146. [[CrossRef](#)]
14. Takeyama, A.; Sugimoto, M.; Yoshikawa, M. Gas permeation property of SiC membrane using curing of polymer precursor film by electron beam irradiation in helium atmosphere. *Mater. Trans.* **2011**, *52*, 1276–1280. [[CrossRef](#)]
15. Völger, K.W.; Hauser, R.; Kroke, E.; Riedel, R.; Ikuhara, Y.H.; Iwamoto, Y. Synthesis and characterization of novel non-oxide sol-gel derived mesoporous amorphous Si–C–N membranes. *J. Ceram. Soc. Jpn.* **2006**, *114*, 567–570. [[CrossRef](#)]
16. Soraru, G.D.; Liu, Q.; Interrante, L.V.; Apple, T. Role of precursor molecular structure on the microstructure and high temperature stability of silicon oxycarbide glasses derived from methylene-bridged polycarbosilanes. *Chem. Mater.* **1998**, *10*, 4047–4054. [[CrossRef](#)]
17. Liu, Q.; Shi, W.; Babonneau, F.; Interrante, L.V. Synthesis of polycarbosilane/siloxane hybrid polymers and their pyrolytic conversion to silicon oxycarbide ceramics. *Chem. Mater.* **1997**, *9*, 2434–2441. [[CrossRef](#)]
18. Lee, L.; Tsai, D.S. A hydrogen-permeable silicon oxycarbide membrane derived from polydimethylsilane. *J. Am. Ceram. Soc.* **1999**, *82*, 2796–2800. [[CrossRef](#)]
19. Hauser, R.; Nahar-Borchard, S.; Riedel, R.; Ikuhara, Y.H.; Iwamoto, Y. Polymer-derived SiBCN ceramic and their potential application for high temperature membranes. *J. Ceram. Soc. Jpn.* **2006**, *114*, 524–528. [[CrossRef](#)]

20. Prasad, R.M.; Iwamoto, Y.; Riedel, R.; Gurlo, A. Multilayer amorphous Si–B–C–N/ γ -Al₂O₃/ α -Al₂O₃ membranes for hydrogen purification. *Adv. Eng. Mater.* **2010**, *12*, 522–528. [[CrossRef](#)]
21. Bazarjani, M.S.; Müller, M.M.; Kleebe, H.-J.; Jüttke, Y.; Voigt, I.; Yazdi, M.B.; Alff, L.; Riedel, R.; Gurlo, A. High-temperature stability and saturation magnetization of superparamagnetic nickel nanoparticles in microporous polysilazane-derived ceramics and their gas permeation properties. *Appl. Mater. Interfaces* **2014**, *6*, 12270–12278. [[CrossRef](#)] [[PubMed](#)]
22. Weinmann, M. Chapter 7 Polysilazanes. In *Inorganic Materials*; De Jaeger, R., Gleria, M., Eds.; Nova Science Publishers Inc.: New York, NY, USA, 2007; pp. 371–413.
23. Iwamoto, Y.; Sato, K.; Kato, T.; Inada, T.; Kubo, Y. A hydrogen-permselective amorphous silica membrane derived from polysilazane. *J. Eur. Ceram. Soc.* **2005**, *25*, 257–264. [[CrossRef](#)]
24. Funayama, O.; Kato, T.; Tashiro, Y.; Isoda, T. Synthesis of a polyborosilazane and its conversion into inorganic compounds. *J. Am. Ceram. Soc.* **1993**, *76*, 717–723. [[CrossRef](#)]
25. Funayama, O.; Tashiro, Y.; Aoki, T.; Isoda, T. Synthesis and pyrolysis of polyaluminosilazane. *J. Ceram. Soc. Jpn.* **1994**, *102*, 908–912. [[CrossRef](#)]
26. Iwamoto, Y.; Kikuta, K.; Hirano, S. Microstructural development of Si₃N₄–SiC–Y₂O₃ ceramics derived from polymeric precursors. *J. Mater. Res.* **1998**, *13*, 353–361. [[CrossRef](#)]
27. Iwamoto, Y.; Kikuta, K.; Hirano, S. Synthesis of poly-titanosilazanes and conversion into Si₃N₄–TiN ceramics. *J. Ceram. Soc. Jpn.* **2000**, *108*, 350–356. [[CrossRef](#)]
28. Kubo, T.; Tadaoka, E.; Kozuka, H. Formation of silica coating films from spin-on polysilazane at room temperature and their stability in hot water. *J. Mater. Res.* **2004**, *19*, 635–642. [[CrossRef](#)]
29. Kubo, T.; Kozuka, H. Conversion of perhydropolysilazane-to-silica thin films by exposure to vapor from aqueous ammonia at room temperature. *J. Ceram. Soc. Jpn.* **2006**, *114*, 517–523. [[CrossRef](#)]
30. Miyajima, K.; Eda, T.; Nair, B.N.; Iwamoto, Y. Organic-inorganic layered membrane for selective hydrogen permeation together with dehydration. *J. Membr. Sci.* **2012**, *421–422*, 124–130. [[CrossRef](#)]
31. Sokri, M.N.M.; Daiko, Y.; Honda, S.; Iwamoto, Y. Synthesis of microporous amorphous silica from perhydropolysilazane chemically modified with alcohol derivatives. *J. Ceram. Soc. Jpn.* **2015**, *123*, 292–297. [[CrossRef](#)]
32. Sokri, M.N.M.; Onishi, T.; Mouline, Z.; Daiko, Y.; Honda, S.; Iwamoto, Y. Polymer-derived amorphous silica-based inorganic-organic hybrids having alkoxy groups: Intermediates for synthesizing microporous amorphous silica materials. *J. Ceram. Soc. Jpn.* **2015**, *123*, 732–738. [[CrossRef](#)]
33. Seyferth, D.; Wiseman, G.; Prud'homme, C. A liquid silazane precursor to silicon nitride. *J. Am. Ceram. Soc.* **1983**, *66*, C-13–C-14. [[CrossRef](#)]
34. Silverstein, R.M.; Bassler, G.C.; Morrill, T.C. *Spectrometric Identification of Organic Compounds*, 5th ed.; John Wiley and Sons, Inc.: New York, NY, USA, 1991.
35. Iwamoto, Y.; Matsunaga, K.; Saito, T.; Völger, W.; Kroke, E.; Riedel, R. Crystallization behaviors of amorphous Si–C–N ceramics derived from organometallic precursors. *J. Am. Ceram. Soc.* **2001**, *84*, 2170–2178. [[CrossRef](#)]
36. Stein, S.E. Mass Spectra in NIST Chemistry WebBook, NIST Standard Reference Database Number 69. Available online: <http://webbook.nist.gov> (accessed on 2 April 2015).
37. Cruz, J.M.D.; Lozovoy, V.V.; Dantus, M. Quantitative mass spectrometric identification of isomers applying coherent laser control. *J. Phys. Chem. Lett. A* **2005**, *109*, 8447–8450.
38. Johnstone, R.A.W. *Mass Spectrometry for Organic Chemists*; Cambridge Chemistry Texts; Cambridge University Press: Cambridge, UK, 1972; pp. 64–67.
39. Watson, J.T.; Sparkman, D. *Introduction to Mass Spectrometry: Instrumentation, Applications, and Strategies for Data Interpretation*, 4th ed.; John Wiley and Sons, Inc.: New York, NY, USA, 2013; pp. 368–376.
40. Sing, K.S.W.; Everett, D.H.; Haul, R.A.W.; Moscou, L.; Pierotti, R.A.; Rouquerol, J.; Siemieniewska, T. Reporting physisorption data for gas/solid systems with special reference to the determination of surface area and porosity. *Pure Appl. Chem.* **1985**, *57*, 603–619. [[CrossRef](#)]
41. Lowell, S.; Shields, J.E.; Thomas, M.A.; Thommes, M. *Characterization of Porous Solid and Powders*; Springer: Dordrecht, The Netherlands, 2004.
42. Breck, D.W. *Zeolite Molecular Sieves*; John Wiley and Sons, Inc.: New York, NY, USA, 1974; p. 636.
43. Li, Y.; Feng, Z.; Lian, Y.; Sun, K.; Zhang, L.; Jia, G.; Yang, Q.; Li, C. Direct synthesis of highly ordered Fe-SBA-15 mesoporous materials under weak acidic conditions. *Microporous Mesoporous Mater.* **2005**, *84*, 41–49. [[CrossRef](#)]

44. Apopei, A.I.; Buzgar, N.; Buzatu, A. Raman and infrared spectroscopy of kaersutite and certain common amphiboles. *AUI Geol.* **2011**, *57*, 35–58.
45. Makreski, P.; Jovanovski, G.; Gajovic, A. Minerals from Macedonia XVII. Vibrational spectra of some common appearing amphiboles. *Vib. Spectrosc.* **2006**, *40*, 98–109. [[CrossRef](#)]
46. Ventura, G.D.; Robert, J.-L.; Beny, J.-M. Tetrahedrally coordinated Ti⁴⁺ in synthetic Ti-rich potassic richterite: Evidence from XRD, FTIR, and Raman studies. *Am. Miner.* **1991**, *76*, 1134–1140.
47. Uchino, T.; Kitagawa, Y.; Yoko, T. Structure, energies, and vibrational properties of silica rings in SiO₂ glass. *Phys. Rev. B* **2000**, *61*, 234–240. [[CrossRef](#)]
48. Matson, D.W.; Sharma, S.K.; Philpotts, J.A. Raman spectra of some tectosilicates and of glasses along the orthoclase-anorthite and nepheline-anorthite joins. *Am. Miner.* **1986**, *71*, 694–704.
49. Kingma, K.J.; Hemley, R.J. Raman spectroscopic study of microcrystalline silica. *Am. Miner.* **1994**, *79*, 269–273.
50. Oyama, S.; Lee, D.; Hacırlıoğlu, P.; Saraf, R.F. Theory of hydrogen permeability in nonporous silica membranes. *J. Membr. Sci.* **2004**, *244*, 45–53. [[CrossRef](#)]
51. Hacırlıoğlu, P.; Lee, D.; Gibbs, G.V.; Oyama, S. Activation energies for permeation of He and H₂ through silica membranes: An *ab initio* calculation study. *J. Membr. Sci.* **2008**, *313*, 277–283. [[CrossRef](#)]
52. Saito, A.; Foley, H. Curvature and parametric sensitivity in models for adsorption in micropores. *AIChE J.* **1991**, *37*, 429–436. [[CrossRef](#)]
53. Barrett, P.; Joyner, G.; Halenda, P.H. The determination of pore volume and area distributions in porous substances. I. Computations from nitrogen isotherms. *J. Am. Chem. Soc.* **1951**, *73*, 373–380. [[CrossRef](#)]



© 2016 by the authors; licensee MDPI, Basel, Switzerland. This article is an open access article distributed under the terms and conditions of the Creative Commons by Attribution (CC-BY) license (<http://creativecommons.org/licenses/by/4.0/>).